

Martin Egli<sup>1</sup>  
Valentina Tereshko<sup>1</sup>  
Marianna Teplova<sup>1</sup>  
George Minasov<sup>1</sup>  
Andrzej Joachimiak<sup>2</sup>  
Ruslan Sanishvili<sup>2</sup>  
Charles M. Weeks<sup>3</sup>  
Russ Miller<sup>3,4</sup>  
Martin A. Maier<sup>5</sup>  
Haoyun An<sup>5</sup>  
P. Dan Cook<sup>5</sup>  
Muthiah Manoharan<sup>5</sup>

<sup>1</sup> Department of Molecular  
Pharmacology  
and Biological Chemistry  
and The Drug Discovery  
Program, Northwestern  
University Medical School,  
Chicago, IL 60611

<sup>2</sup> Structural Biology Center,  
Biosciences Division,  
Argonne National Laboratory,  
Argonne, IL 60439

<sup>3</sup> The Hauptman-Woodward  
Medical Research Institute,  
Buffalo, NY 14203

---

## X-Ray Crystallographic Analysis of the Hydration of A- and B-Form DNA at Atomic Resolution

<sup>4</sup> Department of Computer  
Science and Engineering,  
State University of New York,  
Buffalo, NY 14260

<sup>5</sup> Department of Medicinal  
Chemistry,  
Isis Pharmaceuticals Inc.,  
Carlsbad, CA 92008

Received and accepted 1 November 1999

**Abstract:** We have determined single crystal structures of an A-DNA decamer and a B-DNA dodecamer at 0.83 and 0.95 Å, respectively. The resolution of the former is the highest reported thus far for any right-handed nucleic acid duplex and the quality of the diffraction data allowed determination of the structure with direct methods. The structures reveal unprecedented details of DNA fine structure and hydration; in particular, we have reexamined the overall hydration of A- and B-form DNA, the distribution of water around phosphate groups, and features of the water structure that may underlie the B to A transition. © 2000 John Wiley & Sons, Inc. *Biopoly* 48: 234–252, 1998

**Keywords:** A-DNA; B-DNA; direct methods; hydration; structural transition; water structure; x-ray crystallography

---

Correspondence to: M. Egli; e-mail: m-egli@nwu.edu  
Contract grant sponsor: Department of Energy (DOE) Office of Health and Environmental Research, National Institutes of Health (NIH), and National Science Foundation (NSF)  
Contract grant number: W-31-109-Eng-38 (DOE), GM-46733 and GM-55237 (NIH), ACI-9721373 (NSF)  
*Biopolymers* (Nucleic Acid Sciences), Vol. 48, 234–252 (1998)  
© 2000 John Wiley & Sons, Inc.

## INTRODUCTION

Nucleic acid structure, stability, and recognition are greatly affected by *it* and *it* triggers structural transitions between different duplex forms. *It* is also a key player in the packing of DNA and RNA, and thus the formation of the crystals that have proven so helpful in the studies of *its* many roles. *It*, of course, is water, and the structural transitions include the one between A-form and B-form DNA that is dependent on relative humidity and the nature and concentration of counter ions.<sup>1</sup> The results of the pioneering fiber diffraction studies have long since been superseded by those of single crystal x-ray diffraction analyses of double helical DNA fragments (reviewed in Refs. 2–5) and subsequent insights from their solvent environments (reviewed in Refs. 6–8). The x-ray crystallographic results are complemented by those from studies using solution nmr,<sup>9,10</sup> neutron scattering,<sup>11,12</sup> computational simulation,<sup>13,14</sup> and a host of other techniques.<sup>15,16</sup>

Progress in the understanding of DNA hydration at the atomic level was generally dependent on improvements in the resolutions of oligonucleotide crystal structures. The first single crystal structure of a B-DNA, the Dickerson–Drew dodecamer, revealed a spine of hydration in the minor groove.<sup>17,18</sup> Further regular water networks and bridges were also found for A-form DNA<sup>19–21</sup> and the left-handed Z-DNA.<sup>22,23</sup> The hydration of nucleic acid bases was found to be modular,<sup>24,25</sup> generating predictive patterns in the distribution of water molecules around nucleic acid duplexes.<sup>26</sup> Owing to the higher flexibility of the phosphate groups relative to bases and sugars, the hydration of the charged nucleic acid backbone appears to be less ordered by comparison.<sup>27</sup> The hydration of phosphate groups may be correlated with the distances between them and thus the overall conformation of the double helix.<sup>28</sup> Thus, the 7 Å spacing of adjacent intrastrand phosphate groups in B-DNA precludes formation of single-water bridges. In A-form DNA, the corresponding distance is reduced to around 5.5 Å and a single water can hydrogen bond to both phosphate groups. More systematic arrangements of water molecules involving backbone atoms in Z-DNA structures with resolutions of around 1 Å<sup>23</sup> and in a 1.4 Å structure of an A-form RNA duplex<sup>29</sup> suggested that crystal structures of A- and B-form oligodeoxynucleotide duplexes at very high resolutions might eventually shed light on aspects of hydration that were previously somewhat ill-defined.

We recently refined the crystal structure of the Dickerson–Drew B-DNA dodecamer based on diffraction data collected to 1.1 Å resolution.<sup>30</sup> Analysis

of the structure revealed a large number of additional water molecules compared with earlier studies and the formation of regular water hexagons in both grooves. A 1.2 Å structure of the same dodecamer crystallized in the presence of Rb<sup>+</sup> was used to investigate whether monovalent metal cations can indeed penetrate the minor-groove water spine.<sup>31</sup> The results of this study suggested that the coordination of alkali metal ions to A-tract base functions in the minor groove is an isolated and sequence-dependent event, consistent with earlier molecular dynamics simulations<sup>32,33</sup> and very recent solution nmr work.<sup>34</sup> These structures of the dodecamer grown in the presence of Mg<sup>2+</sup> together with the 1.3 Å structure of a new Ca<sup>2+</sup> form also provided information on the coordination of a total of 12 divalent metal ions to the B-form DNA duplex.<sup>35</sup>

Such advances in the resolution of nucleic acid crystal structures can be achieved thanks to the high intensity of x-ray beams at third-generation synchrotrons, flash freezing of crystals prior to data collection, and constant cooling during data acquisition as well as better methods for synthesizing and purifying DNA. Additional examples are the crystal structure of a parallel-stranded guanine tetraplex determined to 0.95 Å resolution,<sup>36</sup> the crystal structure of a B-DNA nonamer at 0.9 Å resolution<sup>37</sup> and the crystal structure of a B-DNA decamer at 1.15 Å resolution.<sup>38</sup>

Crystallographic work on nucleic acid analogues in our laboratory suggests that chemical modification occasionally improves the chances for growing crystals of an oligonucleotide or leads to better quality of the crystals.<sup>39,40</sup> Thus, our first high-resolution structures of the Dickerson–Drew dodecamer were performed with crystals of an oligonucleotide that contained a single 2'-deoxy-2'-fluoroarabino-thymine.<sup>30,41</sup> However, data with similar resolutions were subsequently obtained from crystals that were grown with native DNA and crystal engineering proved more helpful for maximizing the resolution of the Ca<sup>2+</sup> form than chemical modification.<sup>35</sup> Nevertheless, we are convinced that, provided the effects of a chemical modification in regard to thermodynamic stability, structure, and solvent environment are sufficiently well understood,<sup>42–47</sup> their demonstrated (*vide infra*) and potential benefits for studies of DNA structure, hydration, and ion coordination easily justify the use of oligonucleotides with (chemical) point mutations.

We have now determined crystal structures of two right-handed DNA double helices to better than 1 Å resolution. The structure of the Dickerson–Drew B-form duplex with sequence CGCGAA<sup>F</sup>TTCGCG was refined to 0.95 Å resolution and the structure of an A-form duplex with sequence GCGTA<sup>M</sup>TACGC was

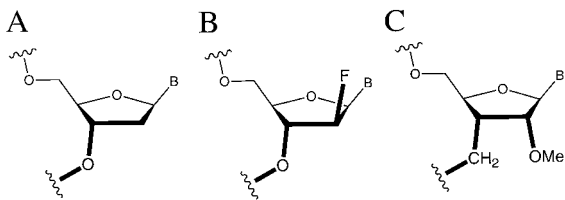


**FIGURE 1** Structure of (A) DNA, (B) 2'-F-ANA, and (C) 2'-MeO-3'MP-DNA.

refined to 0.83 Å resolution. Both duplexes contain a single chemically modified residue per strand. In the case of the dodecamer, <sup>F</sup>T stands for 2'-deoxy-2'-fluoroarabino-T (2'-F-ANA-T, Figure 1) and the <sup>M</sup>T in the decamer represents a 2'-methoxy-3'-methylene-phosphonate-T (2'-MeO-3'MP-T, Figure 1). The structural properties and hydration of 2'-F-ANA-T were previously analyzed in considerable detail.<sup>41</sup> To describe briefly: the modified arabinose sugar adopts an O4'-*endo* pucker that is tolerated within B-form DNA and results in minor structural changes at the local level. Replacement of the bridging phosphate oxygen O3' by a methylene group combined with the methoxy substituent at C2' locks the ribose in a C3'-*endo* pucker, thus stabilizing the overall A geometry of the decamer duplex.<sup>40,48</sup> It is anticipated that replacement of O3' by a methylene group is of little consequence for hydration, since this oxygen is commonly considered a relatively weak acceptor.<sup>27</sup> The structural and hydration features of the 2'-methoxy substituent were analyzed in some detail<sup>49,50</sup> and it is likely to affect DNA hydration only at the local level. Here, we present a preliminary analysis of the two high-resolution structures with a focus on DNA fine structure and hydration.

## METHODS

### Oligonucleotide Synthesis, Purification, and Crystallization

Synthesis and purification of the 2'-F-ANA-modified dodecamer CGCGAA<sup>F</sup>TTCGCG were described previously.<sup>41,51</sup> Crystals were grown in the presence of sodium cacodylate buffer, magnesium acetate, spermine, and 2-methyl-2,4-pentanediol (MPD) precipitant. Details of the crystallization procedure were described elsewhere.<sup>30,31,41</sup> The DNA decamer GCGTA<sup>M</sup>TACGC with a single 2'-MeO-3'MP-thymidine was synthesized using H-phosphonate chemistry and a new method for 3'-methylene phosphonate coupling<sup>52,53</sup> (Isis Pharmaceuticals Inc., to be published). The oligonucleotide was purified by high performance liquid chromatography and ion exchange chromatography. Its pu-

urity was checked with mass spectrometry and capillary gel electrophoresis, and was better than 98%. Crystallization conditions were screened with a sparse matrix kit,<sup>54</sup> using the hanging drop vapor diffusion technique (condition 5). A 4 μL droplet containing 1.25 mM decamer (single strand), 20 mM sodium cacodylate buffer, pH 6.0, 6 mM spermine, 10 mM Mg<sup>2+</sup>, 40 mM K<sup>+</sup> was equilibrated against 1 mL 35% (v/v) MPD. Crystals of the dodecamer and the decamer were mounted in nylon loops, frozen in liquid nitrogen, and then stored in nitrogen before data collection.

### X-Ray Crystallographic Data Collection and Structure Determination

Diffraction data from a single A-DNA crystal were collected on the 5-ID beamline of the DuPont-Northwestern-Dow Collaborative Access Team at the Advanced Photon Source (APS), Argonne National Laboratory, Argonne, Illinois. A total of 660 frames (422,954 reflections) were collected at a wavelength of 0.8000 Å, using three different crystal-detector distances to guarantee optimal completeness of data in the low-, medium-, and high-resolution ranges, and to avoid saturation of high-intensity reflections. Data were processed and merged with the programs DENZO and SCALEPACK,<sup>55</sup> respectively, resulting in 47,403 unique reflections with a completeness of 99.7% to a resolution of 0.83 Å. Selected parameters for quality and amount of data are listed in Table I. Diffraction data from a single B-DNA crystal were collected on the 19-ID beamline of the Structural Biology Center (SBC) at the APS. A total of 560 frames (291,875 reflections) were collected at a wavelength of 0.8152 Å, using two different crystal-detector distances. Data were processed and merged in the HKL2000 suite,<sup>55</sup> resulting in 39,151 unique reflections with a completeness of 94.3% to a resolution of 0.95 Å. Selected parameters for quality and amount of data are listed in Table I.

To our knowledge, no determination of an oligonucleotide crystal structure with direct methods has been reported to date. Conversely, there are quite a few examples of peptides and proteins whose crystal structures were worked out based on the direct-methods approach (for more information, see [http://www.hwi.buffalo.edu/snb/structures\\_snb.htm](http://www.hwi.buffalo.edu/snb/structures_snb.htm)). A basic requirement for successful application of direct methods with macromolecular structures is the availability of diffraction data with sufficiently high resolution, typically higher than 1.2 Å. Motivated by the high resolutions of the diffraction data for the two DNA duplexes, we tested whether direct methods would furnish solutions for their structures.

The A-DNA structure was solved using version 2.0 of the dual-space direct-methods program SnB.<sup>56</sup> The phases of 4250 reflections were refined for 425 cycles using the parameter-shift technique and 42,500 structure-invariant relationships. On account of the presence of the phosphorous atoms, only 170 peaks were selected in each cycle.<sup>57</sup> Six potential solutions out of 3119 trial structures were recognized on the basis of a bimodal minimal-function histogram.

Table I Crystal Data and Refinement Parameters

	A-DNA (GCGTA <sup>M</sup> TACGC)			B-DNA (CGCGAA <sup>F</sup> TTCGCG)		
Crystal data						
Space group	<i>P</i> 2 <sub>1</sub> 2 <sub>1</sub> 2 <sub>1</sub>			<i>P</i> 2 <sub>1</sub> 2 <sub>1</sub> 2 <sub>1</sub>		
<i>a</i> (Å)	24.63			24.62		
<i>b</i> (Å)	42.72			39.73		
<i>c</i> (Å)	46.91			65.74		
V/base pair (Å <sup>3</sup> )	1234			1340		
Data collection and refinement statistics						
X-ray source/detector	5-ID (DNDCAT-APS)/MARCCD			19-ID (SBC-APS)/3 × 3 CCD		
Temperature				120K		
Mosaicity	0.58			0.29		
Resolution (Å)	0.83			0.95		
<i>R</i> <sub>merge</sub> <sup>a</sup>	0.049			0.047		
Resolution range (Å)	<i>N</i> (unique)	%Complete	<i>R</i> Factor <sup>b</sup>	<i>N</i> (unique)	%Complete	<i>R</i> Factor <sup>b</sup>
20–3.0	1130	99.9	0.152	1451	99.6	0.166
3.0–2.5	766	100.0	0.147	1006	100.0	0.164
2.5–2.0	1,735	100.0	0.136	2239	100.0	0.155
2.0–1.5	4742	100.0	0.113	6144	99.9	0.134
1.5–1.3	4331	100.0	0.103	5629	99.9	0.145
1.3–1.1	8040	100.0	0.091	10,478	100.0	0.164
1.1–1.0	6712	100.0	0.091	8122	93.2	0.225
1.0–.95	4460	99.7	0.106	4082	70.2	0.306
.95–.90	5524	99.8	0.120			
.90–.83	9963	98.8	0.129			
All data	47,403	99.7	0.117	39,151 <sup>c</sup>	94.3	0.160
Nonhydrogen DNA atoms		408			488	
B factors <sup>d</sup>		8(4)			17(4)	
Hydration	1st Shell	2nd Shell		1st Shell	2nd Shell	3rd Shell
No. of waters	127	42		150	72	28
B factors <sup>d</sup>	25(15)	30(15)		40(20)	50(25)	60(20)
No. of ions	2 Mg <sup>2+</sup> , 2 spermines			4 Mg <sup>2+</sup>		
RMS <sup>e</sup> distances (Å)	0.022			0.020		
RMS <sup>e</sup> angles (°)	2.06			1.90		

$$^a R_{\text{merge}} = \frac{\sum_{hkl} \sum_i |I(hkl)_i - \langle I(hkl) \rangle|}{\sum_{hkl} \sum_i \langle I(hkl)_i \rangle}$$

$$^b R \text{ factor} = \frac{\sum_{hkl} |F(hkl)_o - F(hkl)_c|}{\sum_{hkl} F(hkl)_o}$$

<sup>c</sup> To a resolution of 0.95 Å.

<sup>d</sup> Average value with standard deviation in parentheses.

<sup>e</sup> Standard parameters taken from Ref. 60.

One of these trial structures was then subjected to 40 additional cycles of dual-space refinement while selecting 425 peaks in each cycle. This refinement was followed by 40 cycles of Fourier refinement before a Fourier map was manually examined. A complete set of initial coordinates was obtained by superimposing an A-form duplex on fragments and isolated atoms that were part of the direct-methods solution. This was done to save time, and it is

important to note that the remaining atoms could have been located by difference Fourier techniques. A “postmortem” analysis revealed that 260 DNA atoms (out of a total of 408), 20 water molecules, and one Mg<sup>2+</sup> ion were actually present in the original SnB map (Figure 2). Interestingly, most of the atoms belong to bases, although 15 out of a total of 18 phosphorus atoms were also found, consistent with the fact that phosphorus is the strongest scatterer in

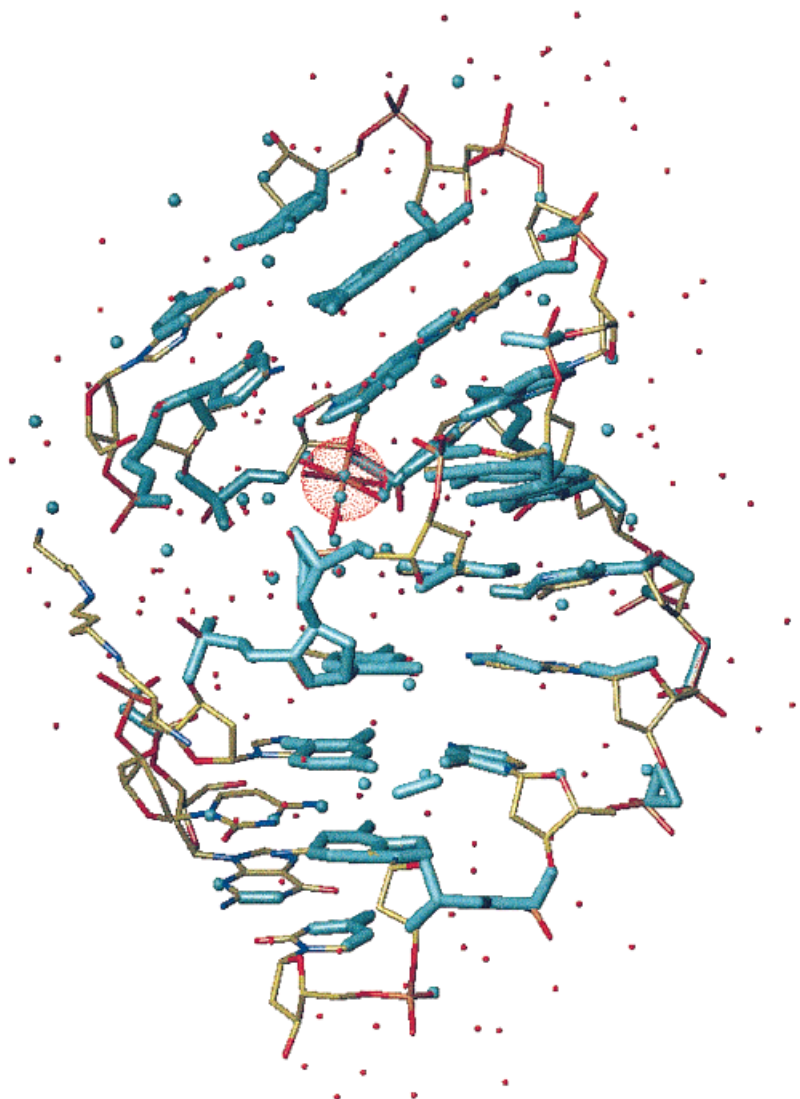


**FIGURE 2** Portions of the A-form duplex and their solvent and ionic environment (in cyan) that were revealed by the direct-methods program SnB superimposed on the final model. DNA atoms are colored yellow, cyan, red, and orange for carbon, nitrogen, oxygen, and phosphorus, respectively; water molecules are small red spheres; the dotted sphere in the center represents a  $Mg^{2+}$  ion; and a spermine molecule is shown at the left.

DNA. However, only few other backbone atoms were present in the original map. This may be a consequence of the higher flexibility of the backbone compared with the base pairs in the core of the duplex. Contrary to the successful determination of the A-DNA crystal structure, direct methods yielded no solution for the structure of the B-form duplex. Therefore, the Nucleic Acid Database<sup>58</sup> entry BD0007, the structure of the identical duplex refined to 1.1 Å resolution,<sup>30</sup> served as the initial model for refinement of the B-DNA dodecamer.

### Structure Refinement

The initial refinements of both structures were carried out with the program CNS<sup>59</sup> using the most recent param-

eter files.<sup>60</sup> In both cases, 10% of the data were set aside for calculating the  $R_{\text{free}}$ .<sup>61</sup> Electron density maps were visualized with the program TURBO FRODO<sup>62</sup> on Silicon Graphics computers. Groups of water molecules were gradually placed in regions of superimposed Fourier sum ( $2F_o - F_c$ ) and difference ( $F_o - F_c$ ) electron density. Anisotropic refinements were then performed with the program SHELX-97.<sup>63</sup> With both structures, all data were included in the final refinement cycles and no sigma cutoffs were used. Final refinement parameters and  $R$  factors are listed in Table I and electron density maps around selected regions of the A-DNA duplex are depicted in Figure 3. These maps reveal clear difference electron density for numerous hydrogen atoms of the nucleic acid bases and in many cases also

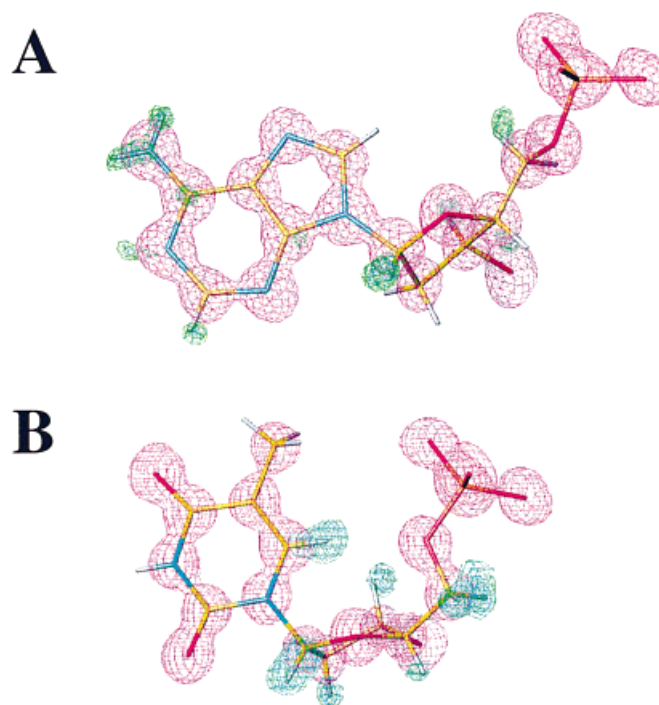


**FIGURE 3** Quality of the electron density around the final model of the A-DNA duplex. ( $2F_o - F_c$ ) sum electron density (magenta), drawn at the  $2\sigma$  level, and ( $F_o - F_c$ ) difference electron density (green and blue), drawn at the  $2.5\sigma$  and  $3\sigma$  level, respectively, around the (A) A5 and (B) T4 nucleotides reveal several of the hydrogen atoms present in the sugar and base moieties. DNA atoms are colored yellow, cyan, red, orange, and light blue for carbon, nitrogen, oxygen, phosphorus, and hydrogen, respectively. Overall, about 60% of all hydrogen atoms are visible in the maps.

for hydrogens in the sugar moieties. For analyzing the structures, nucleotides in the decamer duplex were numbered 1–10 (strand 1) and 11–20 (strand 2), and in the dodecamer, they were numbered 1–12 (strand 1) and 13–24 (strand 2)

### Coordinates

The coordinates and structure factor data for both crystal structures have been deposited with the Protein Data Bank, PDB 1D codes 1DPL (A-decamer) and 1DPN (B-dodecamer).

### OVERALL HYDRATION

Improvements in the resolutions of both structures compared with earlier ones enabled us to locate many more water molecules, belonging to either the first hydration shell or to outer shells, the latter lacking direct contacts to DNA atoms. The asymmetric unit of the A-DNA decamer crystal contains a single duplex, 177 water molecules, 2 spermines, and 2  $Mg^{2+}$  ions. By comparison, only 53 water molecules were found

in the 2.0 Å crystal structure of the A-DNA decamer with sequence GCGTATACGC and a single 2'-methoxy-A per strand.<sup>49</sup> The asymmetric unit of the B-DNA dodecamer crystal contains a single duplex, 250 water molecules, and 4  $Mg^{2+}$  ions. Thus, the number of waters is substantially higher than in the original crystal structure of the dodecamer duplex (72), determined at a resolution of 1.9 Å.<sup>17</sup> The two structures provide a dramatic demonstration of the potential payoffs one can expect from precise measurements of diffraction data to ultrahigh resolution.

To get an overview of the first-shell hydrations of the two DNA duplexes, we generated graphs that illustrate not only the number of hydrogen-bonding partners associated with each potential acceptor and donor in the DNA duplexes, but also allow us to distinguish whether the hydrogen bond is formed to a water molecule or a functional group from a symmetry-related DNA molecule in the crystal lattice (Figure 4). Thus, the graphs provide information about duplex regions involved in close packing contacts in the A- and B-DNA crystal lattices. Lattice interactions in the case of the A-form decamer include stacking of ter-

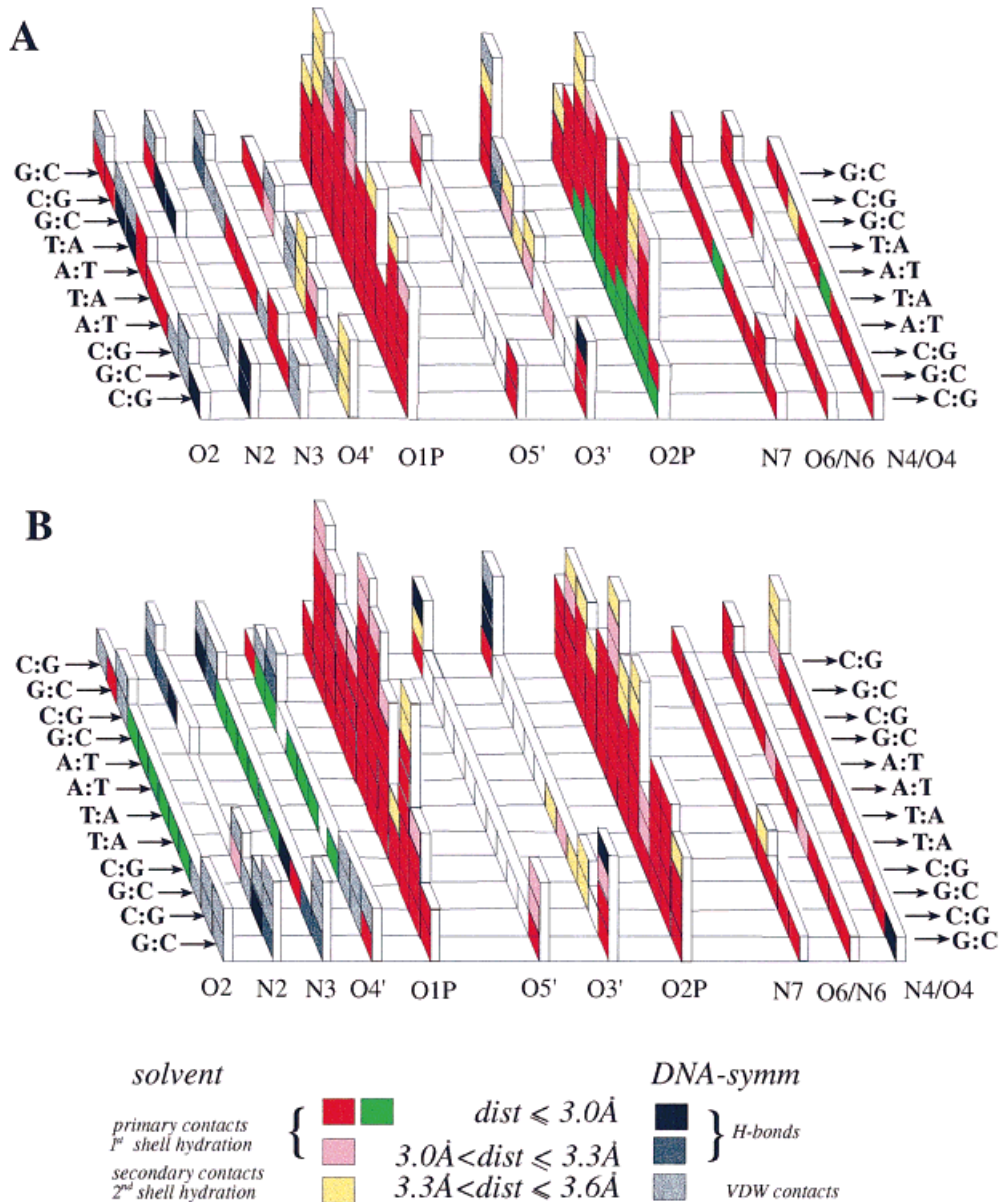


**FIGURE 4** Diagrams illustrating the number and types (water or spermine molecules as well as acceptors or donors from neighboring DNA molecules) of hydrogen-bonding partners as well as the corresponding hydrogen-bond distance ranges (see figure for color code) for individual oxygen and nitrogen atoms in (A) the A-DNA and (B) the B-DNA duplex. Green rectangles represent water molecules that are shared between at least two DNA acceptor atoms, the distances to all of them being shorter than 3 Å (A-DNA: O2P, O4, N7; B-DNA: O4', O2, N3). For all other color codes, see figure and text.

minal base pairs from two duplexes in the minor groove of a third. One consequence of this relatively tight arrangement is the virtual lack of space for formation of a third hydration shell around duplexes (Table I). By comparison, the less tight packing between parallel columns of duplexes in the B-form dodecamer crystal lattice leaves room for a third hy-

dratation shell and the high resolution of the structure enables us to locate many of them (Table I). In the graphs the *x*-axis (horizontal) lists the individual DNA donor and acceptor atoms; minor-groove base and sugar functions are at the left, atoms of the phosphodiester moiety are in the middle, and major-groove base functions are at the right. The individual base pairs are

lined up along the  $y$ -axis and the number of hydrogen-bonding partners corresponds to the height of the column of rectangles, the coloring reflecting the type and the approximate length of the contact (see Figure 4 and legend for details). In this type of analysis, each water molecule is counted only once (represented by one solid rectangle), except in cases where it is shared between two or more DNA atoms and forms hydrogen bonds shorter than 3 Å to all of them (green rectangles, Figure 4). In Figure 4, stronger hydrogen bonds (*primary* contacts) between DNA atoms and water molecules appear as red and pink rectangles, and those between DNA atoms from different duplexes appear as black and grey rectangles. Weaker hydrogen bonds and van der Waals type interactions (*secondary* contacts) appear as yellow and light grey rectangles, respectively.

As can be seen in Figure 4, the largest number of first-shell water molecules in the A- and B-form duplexes are found around phosphate groups. Up to seven waters per base pair lie within a 3 Å range from the O1P and O2P atoms. Secondary contacts of weaker nature are recognizable from yellow or light grey rectangles at the top of the O1P and O2P columns. Conversely, O3' and O5' phosphate ester oxygens are poorly hydrated. For most of them no water molecule lies within a 3 Å distance range and a few O3' atoms constitute secondary partners for water molecules. As expected, the terminal 5'- and 3'-hydroxyl groups are good donors and acceptors, and are surrounded by up to three water molecules. A different picture for the capability of the 4' oxygen to act as a hydrogen bond acceptor emerges for the A- and B-form DNA duplexes. In the A-DNA minor groove, most of the interactions between 4' oxygens and waters or atoms from neighboring DNA molecules appear to be secondary contacts (Figure 4A). In the B-DNA minor groove, the 4' oxygens contribute to the stabilization of the water spine (Figure 4B; Ref. 18 and text below). Although the green rectangles indicate hydrogen bonds with distances <3 Å between O4' atoms and spine waters, each of the latter actually forms four additional strong hydrogen bonds, two to base atoms and two to second-shell waters. Therefore, the hydrogen bonds to O4' can be viewed as secondary contacts by these waters. The O4' atoms of terminal residues in the B-DNA duplex form hydrogen bonds to water molecules that mediate interactions between adjacent duplexes.

An earlier analysis of the hydration of oligonucleotides in crystals found the anionic oxygens of phosphates to be the most hydrated while O5', O3', and O4' were the least hydrated.<sup>64</sup> This relative ranking in terms of the number of hydrogen-bonding contacts

formed by individual DNA atoms remains unchanged at the much higher resolutions of the present structures. What has changed, however, is the number of water molecules that are visible in these structures, furnishing a more complete picture of the first hydration shell and allowing visualization of the solvent networks formed by waters of outer hydration shells.

At the floor of the major and minor grooves, the majority of the purine and pyrimidine base acceptors and donors are engaged in one strong hydrogen bond to either a water molecule or an atom from a neighboring DNA molecule (Figure 4). In the minor grooves of both the A- and the B-DNA duplex, the latter arise as a consequence of interactions between duplexes that comprise base pairs at both ends. However, there are conformation- and crystal lattice-specific patterns in the formation of hydrogen bonds by atoms in the major groove and the minor groove of the A-DNA and B-DNA duplex, respectively. These are analyzed in detail below, along with specific differences of the hydration of the O2P atoms in the A- and B-form duplexes (see color patterns in Figure 4).

## A-DNA MAJOR GROOVE HYDRATION

Analysis of the water structure in the central part of the A-DNA duplex reveals the absence of any contacts to water molecules by the exocyclic amino groups of adenines (Figure 4A, see white rectangles in the N6/O6 row). All other donors and acceptors in the major groove are engaged in a hydrogen bond to a water molecule (Figures 4A, 5A). Close inspection reveals that, among potential hydrogen-bonding partners, the amino groups appear to prefer the O4 oxygen of stacked thymines over water molecules. Considerable negative propeller twisting in A:T base pairs combined with the large slide between adjacent base pairs in an A-form duplex compared with the B-form contribute to a favorable orientation for hydrogen bonds between the N6 donors and the O4 acceptors of stacked bases (Table II). The average distances between N6 and O4 atoms from paired and stacked bases are 3.02 (0.16) and 3.27 (0.15) Å, respectively, and the average O4(paired)–N6–O4(stacked) angle is 109(9)° (standard deviations in parentheses). Obviously, the lack of water around the N6 groups is not a consequence of the presence of the 2'-methoxy groups in T6 and T16 because the substituents are directed into the minor groove. A look at the hydrogen-bonding pattern in the major groove of the B-form duplex shows a different situation, with all exocyclic amino groups of adenines engaged in a hydrogen bond to a water molecule (Figure 4B). Although

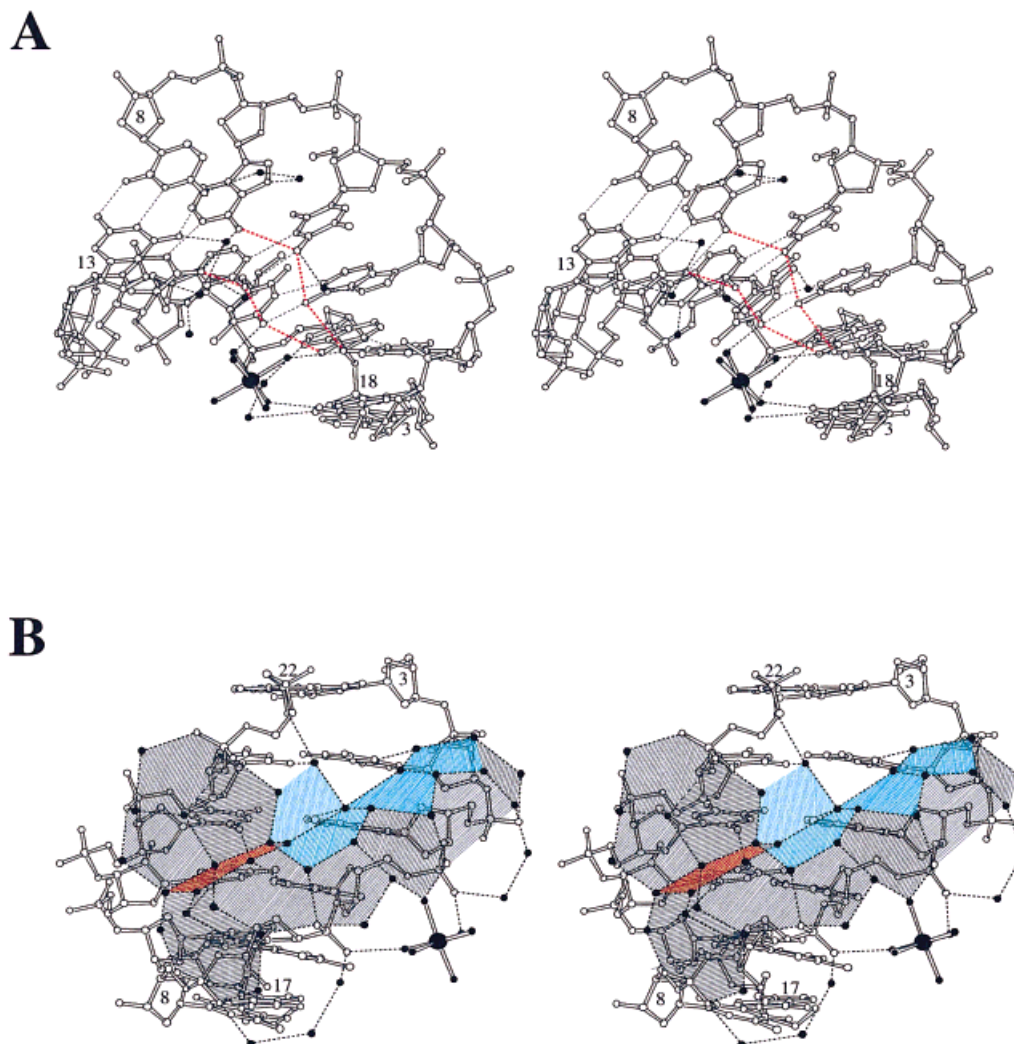


**FIGURE 5** Stereo diagrams of hydration patterns observed in the grooves of the A- and B-DNA duplexes. (A) The six central base pairs in the A-DNA duplex viewed into the major groove; the C8:G13 base pair is at the top and the G3:C18 base pair is at the bottom. The DNA molecule is drawn with open bonds, “bifurcated” hydrogen bonds between N6 of adenosine and O4 of thymine are drawn with red lines. All other hydrogen bonds are drawn with dashed lines, water molecules are small solid circles, and a  $Mg^{2+}$  ion is drawn as a solid circle with a larger radius. (B) Six base pairs of the B-DNA duplex viewed into the minor groove; the C3:G22 base pair is at the top and the T8:A17 base pair is at the bottom. The DNA molecule is drawn with open bonds and a hexagon formed by water molecules from the inner and outer hydration spines is colored in orange (three additional hexagons of this type observed in the minor groove of the A-tract were omitted).<sup>31</sup> Two further ribbons, composed of hexagons and pentagons, are colored in cyan and grey. Hydrogen bonds are drawn with dashed lines, water molecules are small solid circles, and a  $Mg^{2+}$  ion is drawn as a filled circle with a larger radius.

the B-DNA studied here does not contain any TpA steps, it would appear that an A-form geometry is more conducive to formation of good hydrogen bonds between adenine N6 and both O4 atoms from paired and stacked thymines. It is noteworthy that the amino groups of adenines at isolated TpA steps in three other

A-DNA crystal structures at medium resolutions also lack hydrogen bonds to water molecules.<sup>21</sup>

TpA and TpG base steps are known to be rather flexible and to undergo considerable conformational changes at low energy cost.<sup>65</sup> The promoters of prokaryotic and eukaryotic genes feature adjacent TpA

Table II Selected Base Pair and Interbase Pair Parameters in the A-DNA Duplex<sup>a</sup>

Base Pair	Base Pair					Base Pair Step					
	Displacement		Inclin. [°]	Prop. [°]	Buckle [°]	Shift (Å)	Slide (Å)	Rise (Å)	Tilt (°)	Roll (°)	Twist (°)
	<i>x</i> (Å)	<i>y</i> (Å)									
G1:C20	-4.0	0.3	8.1	-9.1	6.3	0.0	-2.0	3.4	1.5	0.0	39.5
C2:G19	-4.0	0.5	7.8	-20.3	2.8	0.4	-2.4	3.3	0.7	5.8	25.9
G3:C18	-3.9	0.0	9.5	-14.2	-3.6	-1.0	-1.8	3.3	-1.6	9.2	36.9
T4:A17	-4.4	0.1	12.3	-14.4	-5.3	0.5	-1.8	3.4	2.0	21.1	28.9
A5:T16	-4.2	-0.1	12.9	-16.5	-5.9	0.9	-1.6	3.2	0.2	6.0	33.9
T6:A15	-3.8	0.0	9.0	-15.7	0.3	-0.1	-1.7	3.1	0.1	12.0	31.1
A7:T14	-4.0	0.1	5.5	-2.8	9.2	-0.3	-2.6	3.4	0.4	5.9	25.7
C8:G13	-4.3	-0.3	3.7	-6.4	9.3	-0.4	-2.4	3.8	-1.0	9.2	31.5
G9:C12	-4.4	-0.4	4.1	-8.4	-8.7	0.0	-2.2	3.3	-0.5	2.2	32.3
C10:G11	-4.4	-0.4	5.1	5.5	-4.5	0.0	-2.2	3.3	-0.5	2.2	32.3
Average:	-4.1	0.0	7.8	-10.3	4.0	0.0	-2.1	3.4	0.2	7.9	31.7

<sup>a</sup> Calculated with the program CURVES.<sup>74</sup>

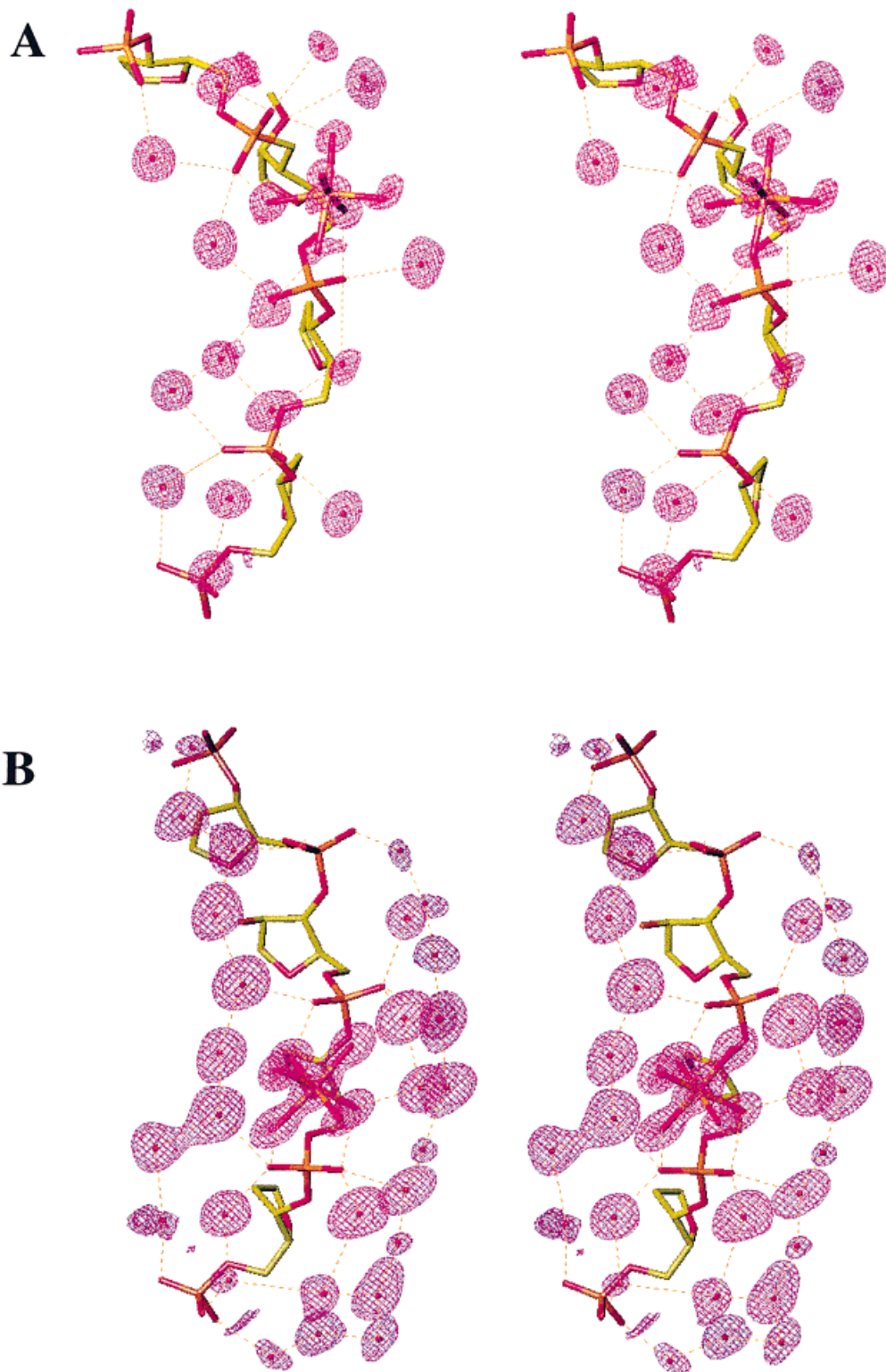
steps, referred to as the TATA box, and TATA-containing oligodeoxynucleotides, crystallized alone or in complex with proteins, exhibit an A-like geometry, now called TA-DNA (Ref. 66 and cited papers). The finding in our structure that adenine N6 at TpA steps is not hydrated is consistent with the favored adoption of an A-conformation by the TATA element. In fact, it may contribute to the apparently facile transition from the B to the A geometry by duplex portions containing multiple TpA steps. It is tempting to speculate that a DNA duplex with multiple TpA steps will readily undergo the transition from B- to A-form in part because the loss of a single water molecule by each A:T base pair is compensated for by an intrastrand base-base hydrogen bond. This, in turn, is consistent with the B- to A-form transition being favored under conditions of low humidity.<sup>1</sup>

A particular feature of the structure of the [d(GCG-TATACGC)]<sub>2</sub> duplex is the kink between base pairs T4:A17 and A5:T16, indicated by a large roll angle between them, along with a considerable tilt and a reduced helical twist (Table II). This geometry may lead to more optimal interactions between duplexes in the crystal lattice, comprising stacking of terminal

base pairs against the shallow minor groove of an adjacent duplex. A Mg<sup>2+</sup> ion that forms an outer sphere complex with the edges of three consecutive base pairs is likely to stabilize the kink in the duplex (Figure 5A). At the periphery of the major groove, fused hexagons and pentagons of water molecules connect the phosphate backbone with the bases (data not shown), an observation that was first made in the crystal structure of the A-DNA octamer GGTATACC at a resolution of 1.7 Å.<sup>19</sup>

## B-DNA MINOR GROOVE HYDRATION

The spine of hydration is a hallmark of the Dickerson-Drew B-DNA dodecamer: A string of water molecules bridges adjacent adenines and thymines from opposite strands at the floor of the minor groove.<sup>17,18</sup> First-shell waters that are part of the spine are shared between two acceptors, typically N3 of A and O2 of T, and at the central ApT step, between O2 atoms of T7 and T19. This is manifested by the series of green rectangles in the central sections of the N3 and O2 rows in Figure 4B. Structures of the dodeca-



mer duplex at resolutions higher than 1.2 Å established an outer spine of waters in the minor groove.<sup>30,31</sup> Together with the above inner spine, the minor groove waters form a ribbon of fused hexagons that dissects the groove along the central GAATTC stretch in the dodecamer duplex (Figure 5B, only one orange hexagon depicted).

The present structure gives a more complete picture of the patterns defined by waters bound to the C:G portions of the duplex. There, fused polygons of waters wind along one border of the groove (Figure 5B, cyan planes). This ribbon involves waters of the first, second, and third shells, and constitutes, in fact, an extension of the water ribbon (orange) in the A-tract of the duplex. Thus, widening of the groove in the outer portions of the duplex causes the water ribbon to turn away from the center of the groove and curve along the backbone, thereby bridging base functions and phosphate oxygens. On the opposite side of the minor groove, interactions between the ends of duplexes (not shown) prevent the formation of this water ribbon and only a number of isolated water molecules are discernible in this region (Figure 5B). However, in the absence of these intermolecular interactions, one can imagine the central ribbon of orange hexagons splitting into two cyan ribbons outside the A-tract, both of which will wind along the backbone.

At the periphery of the minor groove, water hexagons and pentagons are arranged more or less perpendicularly to the two above water ribbons (Figure 5B, grey planes). Water molecules that are part of this network bridge the backbones from opposite strands in the central narrow section of the duplex, thus effectively sealing the minor groove. In the wider outer regions of the duplex, the grey polygons extend the water ribbon that runs along the inside of the groove and wrap around the sugar-phosphate backbone. The B-DNA crystal structure confirms cyclic configurations involving either five or six water molecules as the preferred basic component of solvent networks around DNA, in line with the results of other analyses of the water structure around pro-

teins,<sup>67</sup> oligonucleotides<sup>19,29,68</sup> and small peptides.<sup>69</sup> It also establishes the well-known spine of hydration as just a well ordered fragment of a more extensive solvent network that fills the entire groove and creates a web around the DNA.

## PHOSPHATE HYDRATION

Comparison of the number of hydrogen-bonding contacts by phosphate groups shows that O1P oxygens are somewhat better hydrated in the B-form than in the A-form duplex (Figure 4). As mentioned before, several O3' phosphate oxygens are engaged in secondary contacts. The number of hydrogen bonds to 3' oxygens in the 3.0–3.3 Å distance range is somewhat higher in the A-DNA duplex. By comparison, bridging 5' oxygens are not engaged in any contacts to water that are shorter than 3.6 Å. The hydration of O2P oxygens is conformation dependent, as manifested by a total of 12 green rectangles in the O2P row of the A-DNA hydration graph shown in Figure 4A. Each of these represents a water molecule that is shared between two adjacent intrastrand O2P oxygens. The relatively short distance between adjacent phosphates in A-DNA compared with B-DNA allows overlaps between the hydration shells of individual phosphate groups. In B-DNA, where adjacent phosphate groups are separated by about 7 Å, single water molecules cannot bridge them. Such phosphate groups in the A-form duplex are typically bridged by one (O2P) or two (O1P) water molecules (Figure 6A). Conversely, in the B-form duplex, adjacent phosphates are bridged by two, three or more water molecules (Figures 5B, 6B).

Overall, the trends for water-phosphate interactions observed in the two high-resolution structures here are consistent with those of a recent exhaustive overview of phosphate hydration in DNA.<sup>27</sup> Thus, the extent of hydration around phosphate groups is clearly larger than around bases (Figure 3). Although the water structure around bases is more ordered than around phosphates, many more water molecules can

**FIGURE 6** Hydration of phosphate groups in A- and B-DNA. (A) Portion of the A-DNA backbone between residues T14 (bottom) and A17 (top). The 2'MeO-3'MP-modified residue T16 and a water coordinated to its 2' oxygen are visible at the upper right, next to the Mg<sup>2+</sup> ion. (B) Portion of the B-DNA backbone between residues A5 (bottom) and C9 (top). The 2'F-ANA residue is visible near the top and a hydrated Mg<sup>2+</sup> ion is located between its phosphate and that of residue A6. No distortion of the water structure around the DNA is observed as a consequence of the modified residue. ( $2F_o - F_c$ ) omit electron density ( $2\sigma$  level) around water molecules is shown in magenta. DNA atoms are colored yellow, red, and orange for carbon, oxygen, and phosphorus, respectively; water molecules are small red spheres and hydrogen bonds are dashed lines.

be observed around the backbones in the two structures compared to earlier ones with lower resolutions. This suggests that only few water molecules that are bound to phosphates and are part of the first and second hydration shells can still not be visualized in the electron density maps. Therefore, any further improvements should not significantly alter the picture of phosphate hydration that emerges from the present atomic-resolution data. Another earlier observation that is borne out by the two structures is the more economical hydration of the A-DNA backbones compared with B-DNA.<sup>28</sup> A conformation that allows single water molecules to bridge neighboring phosphate groups should be preferred at low water activity and hence the transition from the B- to the A-conformation at low humidity, as originally observed with crystalline fibers.<sup>1</sup>

## BACKBONE FLEXIBILITY

The sugar–phosphate backbone of the A-DNA duplex exhibits local conformational flexibility in the crystal structure discussed here. Around nucleotides A7 and C8 as well as in the region of C18 and G19, electron density maps reveal two discrete geometries for parts of the backbone and the sugars (Figure 7). Therefore, the positions of atoms associated with the two conformations along with several water molecules hydrogen bonded to phosphate oxygens were refined with partial occupancies. In the case of the first strand, the backbone disorder is associated with a concomitant change of the  $\alpha$  and  $\gamma$  torsion angles of C8 from a *–sc* to an *ap* conformation, resulting in a 1.25 Å shift of the phosphate group (Table III, Figure 7A). This flipping of the  $\alpha, \gamma$  pair is the product of a crankshaft motion around the O5'—C5' bond (torsion angle  $\beta$ ), creating the well-known and quite common extended backbone variant of the A-DNA backbone.<sup>70</sup> Further changes in A7 and C8 concern the sugar pucker of both residues, with the pseudorotation phase angles deviating by ca. 7° between the alternative backbone conformations (Table III). However, the orientations of the bases are invariant and there are only very minor changes in the glycosidic torsion angles for the two residues (Figure 7A, Table III). In addition, the backbone torsion angles on the 3'-side of residues A7 and C8 ( $\epsilon$  and  $\zeta$ ) remain virtually unaffected by the change from one conformation to the other.

A somewhat similar picture emerges for the site of backbone disorder in the second strand. Compared with C8, the geometric variations of the backbone in G19 involve smaller changes in the conformations of

torsion angles  $\alpha$  and  $\gamma$ . Contrary to the situation in the first strand, residue G19 adopts an extended conformation in both arrangements of the backbone. The switch from one conformation to the other also involves a 10° change in its glycosidic angle (Figure 7B, Table III). Conformational flexibility of the backbone was also observed in the structure of the B-DNA duplex (Figure 8). However, the ensuing changes in the conformations of various backbone angles are more subtle compared with the A-DNA duplex and amount to rather small changes in the orientations of phosphate groups.

## THERMAL MOTION AND VALENCY OF WATER MOLECULES

An analysis of the thermal motions of the DNA duplex and water molecules in the two crystal lattices reveals no surprises in the case of DNA atoms. Average values for *B* factors of DNA atoms and water molecules belonging to individual shells are given in Table I. Graphic representations of the thermal motions of individual DNA moieties and selected groups of water molecules are depicted in Figure 9. Accordingly, phosphate groups display the highest flexibility and the stacked bases are the least flexible among DNA atoms (Figure 9). Second- and third-shell water molecules have higher *B* factors compared with those constituting the first hydration shell. The thermal parameters of the latter reflect particular topological features of the A- and B-form duplexes. For example, waters hydrogen bonded to O2P oxygens in the deep major groove of A-DNA have an average *B* factor of  $19 \pm 10 \text{ \AA}^2$ . Those hydrogen bonded to the more exposed O1P oxygens have an average *B* factor of  $32 \pm 23 \text{ \AA}^2$  (Figure 9). In the B-form duplex, waters bound to O1P or O2P oxygens display similar average *B* factors ( $44 \pm 19$  and  $42 \pm 21 \text{ \AA}^2$ , respectively). In both structures, the average *B* factor of first-shell water molecules that reside in the minor groove is slightly lower than the one of major groove waters (Figure 9).

To check whether some water molecules might in fact be sodium ions, the coordination geometries of all waters in the two structures were examined and their valences were calculated based on the parameters for Na<sup>+</sup> published in Ref. 71. The ideal distance between Na<sup>+</sup> and oxygen is around 2.4 Å and thus about 0.3–0.5 Å shorter than a typical hydrogen bond. Moreover, the theoretical valence of a sodium ion is 1 and water molecules whose valences approach this value therefore may represent ions.<sup>72,73</sup> The average valences of water molecules belonging to the first,

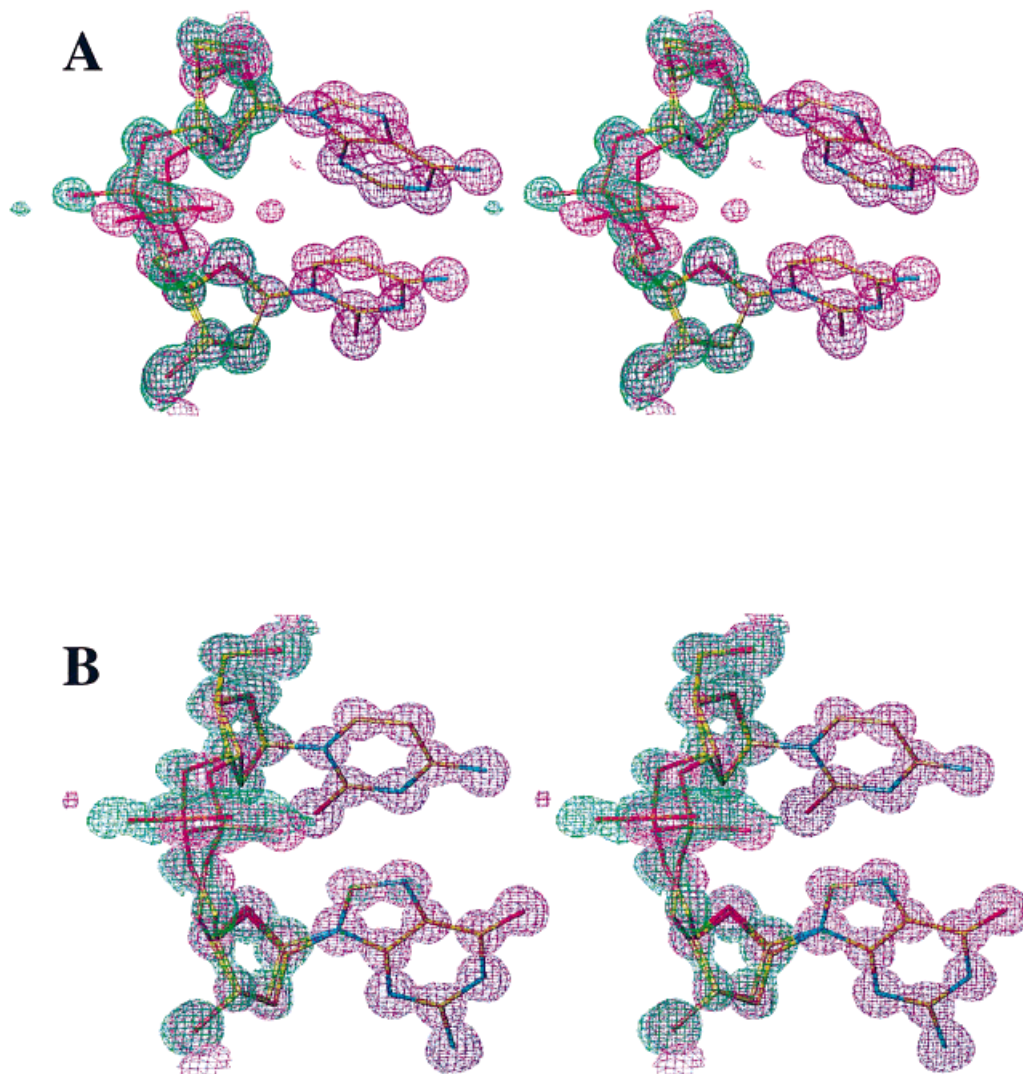


**FIGURE 7** Local conformational flexibility of the A-DNA backbone: Stereo diagram of two alternative conformations adopted by the sugar–phosphate backbone (A) around nucleotides A7 and C8 and (B) around nucleotides C18 and G19. ( $2F_o - F_c$ ) sum electron density ( $2\sigma$  level) for one arrangement is shown in magenta and ( $F_o - F_c$ ) omit electron density ( $3\sigma$  level) for the other is shown in green. DNA atoms are colored yellow, cyan, red, and orange for carbon, nitrogen, oxygen, and phosphorus, respectively. The colors of electron densities for water molecules hydrogen bonded to phosphate oxygens that belong to alternative conformations match those around the corresponding backbones.

second, and third hydration shells are plotted in Figure 10. None of the calculated values was indicative of an ion and, interestingly, the average valences of first- and second-shell water molecules are very similar, both in the structure of the A- and the B-form duplex. The fact that this approach failed to point out potential ion coordination sites should by no means be taken as an indication that there are no sodium ions present in these crystals. However, alternative methods, such as cocrystallization of DNA with heavier

alkali metal ions, may be used to shed light on ion coordination (Ref. 31 and cited papers).

## CONCLUSIONS AND OUTLOOK

The two high-resolution structures of A- and B-form duplexes have confirmed many previous observations concerning the hydration of DNA, including

**Table III** Local Conformational Flexibility of the A-DNA Backbone<sup>a</sup>

Conf.	Residue	Torsion Angles (°), Pseudorotation Phase Angle <i>P</i> (°), and Sugar Pucker								
		$\chi$	$\alpha$	$\beta$	$\gamma$	$\delta$	<i>P</i>	Pucker	$\epsilon$	$\zeta$
1	A7	-157.4	-71.4	-177.1	48.3	79.2	6.8	C3'-endo	-160.2	-69.6
1	C8	-167.6	-64.5	169.0	60.1	75.6	21.9	C3'-endo	-162.6	-68.1
2	A7	-155.6	-71.4	-177.1	69.2	78.9	30.6	C3'-endo	-169.1	-63.8
2	C8	-168.0	148.5	-176.5	177.0	79.4	356.5	C2'-exo	-158.2	-61.1
1	C18	-161.6	-68.8	-179.3	49.6	74.1	11.5	C3'-endo	179.2	-74.5
1	G19	-177.0	-167.4	-150.5	145.8	83.4	5.7	C3'-endo	-137.9	-68.1
2	C18	-161.5	-70.2	-179.3	58.4	84.1	20.3	C3'-endo	-166.6	-66.7
2	G19	-168.7	147.7	-171.4	-176.4	97.8	351.5	C2'-exo	-144.7	-67.6

<sup>a</sup> All parameters were calculated with the program CURVES.<sup>74</sup>

the conformation dependence of the water structure surrounding the sugar-phosphate backbone. Fewer waters are necessary to hydrate the closely spaced phosphate groups in A-DNA compared with the need for individual hydration shells around phosphate groups in the extended backbone of B-DNA. Therefore, low water activity will shift the conformational equilibrium between the two fundamental duplex geometries toward the A-form. However, the structure of the A-DNA decamer duplex has also revealed a previously not noticed aspect of TpA steps. In the

major groove of such steps, exocyclic N6 amino groups of adenines are not just engaged in a hydrogen bond to the O4 keto oxygen of a paired thymine, but in addition, are hydrogen bonding to the O4 oxygen of the stacked T. In view of the specific biological role played by TpA steps in the promoters of prokaryotic and eukaryotic genes, this is quite an intriguing finding. It further highlights the conformational uniqueness of the TpA step and lends support to the notion that DNA regions containing consecutive TpA steps prefer an A-like conformation.

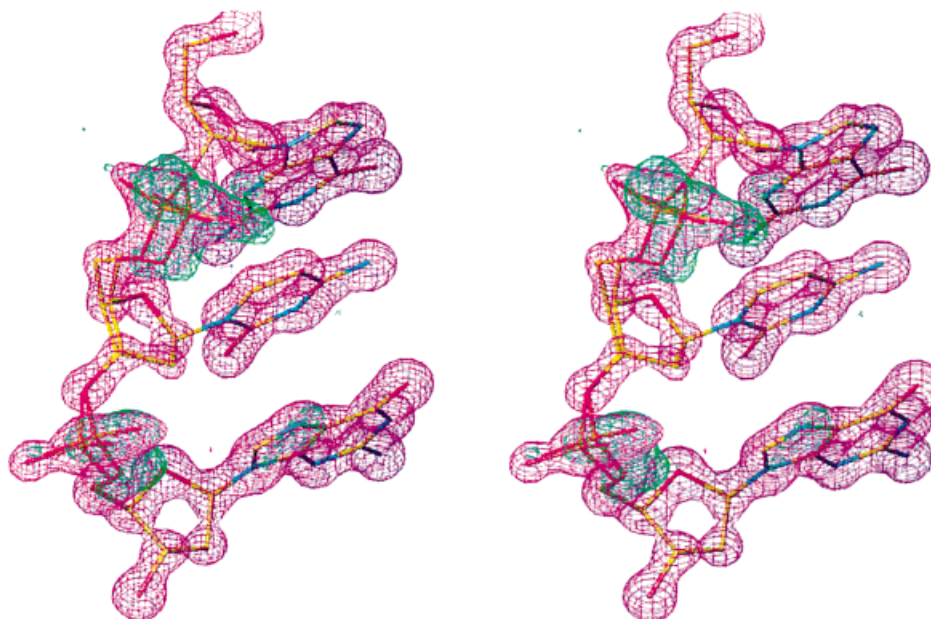


**FIGURE 8** Local conformational flexibility of the B-DNA backbone: Stereo diagram of two alternative conformations adopted by the phosphate groups of nucleotides C23 (center) and G24 (top). ( $2F_o - F_c$ ) sum electron density ( $2\sigma$  level) for one arrangement is shown in magenta and ( $F_o - F_c$ ) omit electron density ( $3\sigma$  level) for the other is shown in green. DNA atoms are colored yellow, cyan, red, and orange for carbon, nitrogen, oxygen, and phosphorus, respectively.

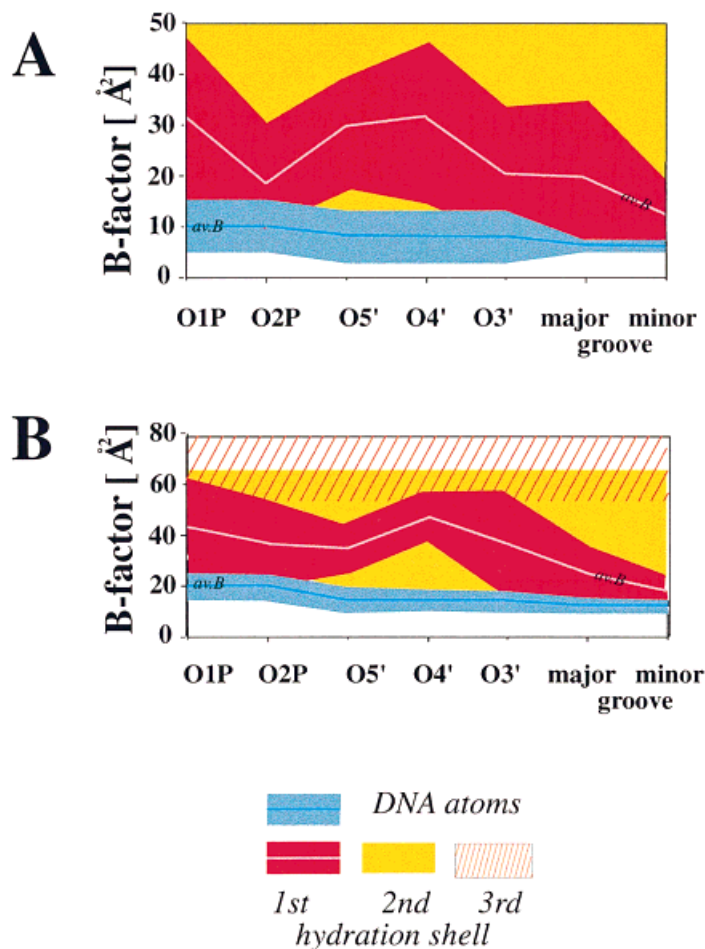


**FIGURE 9** Thermal motions of DNA atoms and water molecules in (A) the A-DNA structure and (B) the B-DNA structure. For individual DNA atoms and first-shell water molecules hydrogen bonded to them, the widths of the areas above and below the average correspond to the standard deviations. In the case of the second and third hydration shells, the width of the ribbon indicates the range of the observed  $B$  factors for water molecules. The color code is as follows: Red for DNA atoms (pink line: average  $B$  factor), blue for first-shell water molecules (cyan line: average  $B$  factor), yellow for second-shell water molecules, and area shaded in red for third-shell water molecules (B-DNA only).

While many other crystal structures provided insight into the first and second hydration shells around DNA, the present structures give a more complete picture of the DNA water structure. The majority of first and second shell waters are observed and in the B-DNA crystal structure many waters belonging to the third shell are now also visible. Therefore, the two structures can serve as more reliable experimental standards, e.g., for the purpose of comparisons with computationally simulated arrangements of water around double-helical DNA. While we have clearly come a long way in terms of the precision of x-ray crystal structures of nucleic acids, it is obvious that further technological advances will result in addi-

tional improvements in the near future. Thus, it is conceivable that we will obtain crystal structures of DNA duplexes that will match the resolution and precision of current small molecule structures. Although we now have a much more detailed conception of the water structure around DNA, much remains to be learnt about the coordination of ions, particularly monovalent metal cations, to DNA. Thus, even at the very high resolutions of the two structures reported here, the combined positive charges of the observed cations only account for the neutralization of 12 (out of 18) and 8 (out of 22) phosphate groups in the A- and B-DNA duplexes, respectively. It is possible that some of the positive

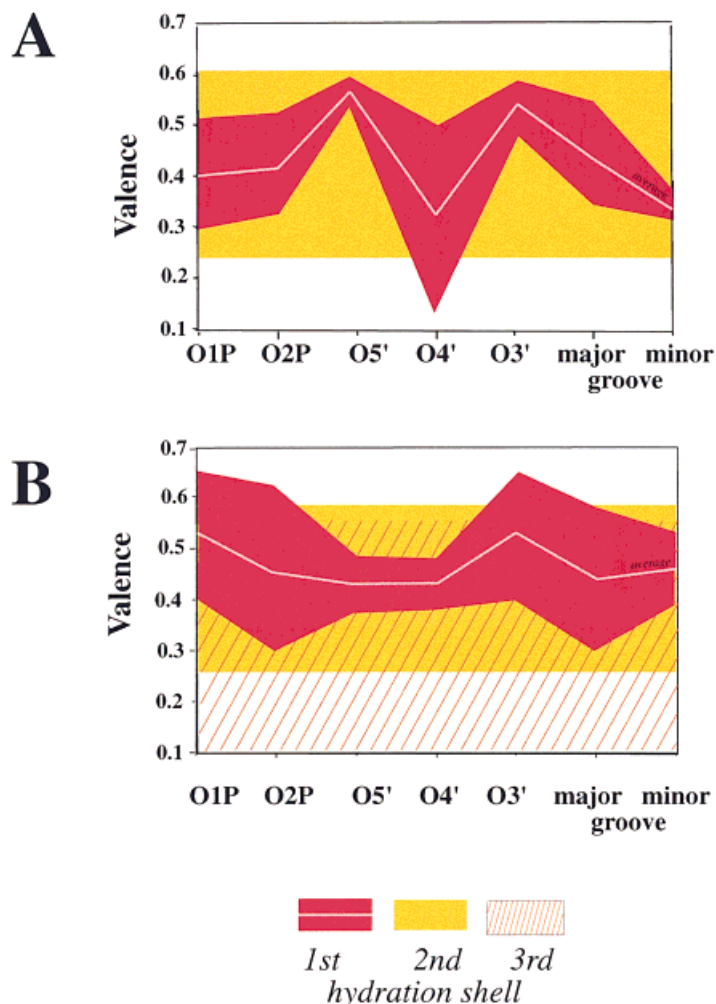


**FIGURE 10** Valences of first-, second-, and third-shell (B-DNA only) water molecules in (A) the A-DNA structure and (B) the B-DNA structure. For first-shell water molecules, the widths of the areas above and below the average correspond to the standard deviations. In the case of the second and third hydration shells, the width of the ribbon indicates the range of the calculated valences for water molecules. The color code is as follows: Red for first-shell water molecules (pink line: average valence), yellow for second-shell water molecules, and area shaded in red for third-shell water molecules.

charges are contributed by alkali metal ions that are weakly coordinated to the DNA or are residing in the outer hydration shells and are thus more flexible. We hope that ultrahigh-resolution structures of DNA duplexes crystallized in the presence of  $K^+$ ,  $Rb^+$ , or  $Cs^+$  ions and their comparisons with a reference structure (crystallized in the presence of  $Na^+$ ) will eventually yield information on the whereabouts of the elusive metal ions.

This research was supported by the Department of Energy Office of Health and Environmental Research Contract W-31-109-Eng-38 (to AJ), the National Institutes of Health (GM-46733 to CMW and RM, and GM-55237 to ME), and

the National Science Foundation (ACI-9721373 to CMW and RM). Computing time for the SnB program was provided by the Center for Computational Research at SUNY Buffalo and by the SnB Alpha server at the Hauptman-Woodward Institute. The DuPont-Northwestern-Dow Collaborative Access Team Synchrotron Research Center at the Advanced Photon Source, Argonne, Illinois, is supported by E. I. DuPont de Nemours & Co., The Dow Chemical Company, the National Science Foundation, and the State of Illinois.

## REFERENCES

1. Franklin, R. E.; Gosling, R. G. *Nature* 1953, 171, 740-741.

2. Saenger, W. Principles of Nucleic Acid Structure; Springer Verlag: New York, 1984.
3. Kennard, O.; Hunter, W. N. *Angew Chem Int Ed Engl* 1991, 30, 1254–1277.
4. Dickerson, R. E. *Methods Enzymol* 1992, 211, 67–111.
5. Egli, M. In *Structure Correlation*; Bürgi, H.-B., Dunitz, J. D., Eds.; VCH Publishers: Weinheim, Germany, 1994; Vol 2, pp 705–749.
6. Berman, H. M.; Schneider, B. In *Handbook of Nucleic Acid Structure*; Neidle, S., Ed.; Oxford University Press: Oxford, 1999; pp 295–312.
7. Westhof, E. In *Water and Biological Macromolecules*; Westhof, E., Ed.; CRC Press: Boca Raton, FL, 1993; pp 226–243.
8. Jeffrey, G. A.; Saenger, W. *Hydrogen Bonding in Biological Structures*; Springer Verlag: Heidelberg, 1991.
9. Wüthrich, K. *Cold Spring Harbor Symp Quant Biol* 1993, 149–157.
10. Kochoyan, M.; Leroy, J. L. *Curr Opin Struct Biol* 1995, 5, 329–333.
11. Pope, L. H.; Shotton, M. W.; Forsyth, V. T.; Langan, P.; Denny, R. C.; Giesen, U.; Dauvergne, M. T.; Fuller, W. *Phys B* 1997, 241, 1156–1158.
12. Shotton, M. W.; Pope, L. H.; Forsyth, V. T.; Langan, P.; Grimm, H.; Rupperecht, A.; Denny, R. C.; Fuller, W. *Phys B* 1997, 241, 1166–1168.
13. Cheatham, T. E., III; Kollman, P. A. *J Mol Biol* 1996, 259, 434–444.
14. Young, M. A.; Ravishanker, G.; Beveridge, D. L. *Biophys J* 1997, 73, 2313–2336.
15. Chalikian, T. V.; Sarvazyan, A. P.; Plum, G. E.; Breslauer, K. J. *Biochemistry* 1994, 33, 2394–2401.
16. Hummer, G.; Garcia, A. E.; Soumpasis, D. M. *Biophys J* 1995, 68, 1639–1652.
17. Drew, H. R.; Dickerson, R. E. *J Mol Biol* 1981, 151, 535–556.
18. Kopka, M. L.; Fratini, A. V.; Drew, H. R.; Dickerson, R. E. *J Mol Biol* 1983, 163, 129–146.
19. Kennard, O.; Cruse, W. B. T.; Nachman, J.; Prange, T.; Shakked, Z.; Rabinovich, D. *J Biomol Struct Dynam* 1986, 3, 623–647.
20. Eisenstein, M.; Shakked, Z. *J Mol Biol* 1995, 248, 662–678.
21. Tippin, D. B.; Sundaralingam, M. *Biochemistry* 1997, 36, 536–543.
22. Chevrier, B.; Dock, A. C.; Hartmann, B.; Leng, M.; Moras, D.; Thuong, M. T.; Westhof, E. *J Mol Biol* 1986, 188, 707–719.
23. Gessner, R. V.; Quigley, G. J.; Egli, M. *J Mol Biol* 1994, 236, 1154–1168.
24. Schneider, B.; Cohen, D.; Berman, H. M. *Biopolymers* 1992, 32, 725–750.
25. Schneider, B.; Berman, H. M. *Biophys J* 1995, 69, 2661–2669.
26. Schneider, B.; Cohen, D. M.; Schleifer, L.; Srinivasan, A. R.; Olson, W. K.; Berman, H. M. *Biophys J* 1993, 65, 2291–2303.
27. Schneider, B.; Patel, K.; Berman, H. M. *Biophys J* 1998, 75, 2422–2434.
28. Saenger, W.; Hunter, W. N.; Kennard, O. *Nature* 1986, 324, 385–388.
29. Egli, M.; Portmann, S.; Usman, N. *Biochemistry* 1996, 35, 8489–8494.
30. Tereshko, V.; Minasov, G.; Egli, M. *J Am Chem Soc* 1999, 121, 470–471.
31. Tereshko, V.; Minasov, G.; Egli, M. *J Am Chem Soc* 1999, 121, 3590–3595.
32. Young, M. A.; Jayaram, B.; Beveridge, D. L. *J Am Chem Soc* 1997, 119, 59–69.
33. Young, M. A.; Jayaram, B.; Beveridge, D. L. *Biophys J* 1997, 73, 2313–2336.
34. Denisov, V. P.; Halle, B. *Proc Natl Acad Sci USA* 1999, submitted.
35. Minasov, G.; Tereshko, V.; Egli, M. *J Mol Biol* 1999, 291, 83–99.
36. Phillips, K.; Dauter, Z.; Murchie, A. I. H.; Lilley, D. M. J.; Luisi, B. *J Mol Biol* 1997, 273, 171–182.
37. Soler-Lopez, M.; Malinina L.; Liu, J.; Hyunh-Dinh, T.; Subirana, J. A. *J Biol Chem* 1999, 274, 23683–23686.
38. Vlieghe, D.; Turkenburg, J. P.; Van Meervelt, L. *Acta Cryst D* 1999, 55, 1495–1502.
39. Egli, M. *Angew Chem Int Ed Engl* 1996, 35, 1894–1909.
40. Egli, M. In *Advances in Enzyme Regulation*; Weber, G., Ed.; Elsevier Science: Oxford, UK, 1998; Vol 38, pp 181–203.
41. Berger, I.; Tereshko, V.; Ikeda, H.; Marquez, V. E.; Egli, M. *Nucleic Acids Res* 1998, 26, 2473–2480.
42. Portmann, S.; Altmann, K.-H.; Reynes, N.; Egli, M. *J Am Chem Soc* 1997, 119, 2396–2403.
43. Egli, M. *Antisense Nucleic Acid Drug Develop* 1998, 8, 123–128.
44. Tereshko, V.; Gryaznov, S.; Egli, M. *J Am Chem Soc* 1998, 120, 269–283.
45. Tereshko, V.; Portmann, S.; Tay, E.; Martin, P.; Natt, F.; Altmann, K.-H.; Egli, M. *Biochemistry* 1998, 37, 10626–10634.
46. Teplova, M.; Minasov, G.; Tereshko, V.; Inamati, G. B.; Cook, P. D.; Manoharan, M.; Egli, M. *Nature Struct Biol* 1999, 6, 535–539.
47. Teplova, M.; Wallace, S. T.; Minasov, G.; Tereshko, V.; Symons, A.; Cook, P. D.; Manoharan, M.; Egli, M. *Proc Natl Acad Sci USA* 1999, 96, 14240–14245.
48. Egli, M.; Usman, N.; Rich, A. *Biochemistry* 1993, 32, 3221–3237.
49. Lubini, P.; Zürcher W.; Egli, M. *Chem Biol* 1994, 1, 39–45.
50. Adamiak, D. A.; Milecki, J.; Popena, M.; Adamiak, R. W.; Dauter, Z.; Rypniewski, W. R. *Nucleic Acids Res* 1997, 25, 4599–4607.

51. Ikeda, H.; Fernandez, R.; Wilk, A.; Barchi, J. J., Jr.; Marquez, V. E. *Nucleic Acids Res* 1998, 26, 2237–2244.
52. An, H.; Wang, T.; Maier, M. A.; Haly, B. D.; Bharadwaj, R.; Cummins, L. L.; Owens, S.; Lesnik, E.; Wheeler, P.; Manoharan, M.; Ross, B.; Freier, S.; Cook, P. D. *Abstr Am Chem Soc CARB 0092*, 218th Am Chem Soc Meeting, New Orleans, LA, 1999. p 73.
53. Maier, M. A.; Guzaev, A. P.; Wheeler, P.; An, H.; Wang, T.; Cook, P. D.; Manoharan, M. *Abstr Am Chem Soc CARB 0091*, 218th Am Chem Soc Meeting, New Orleans, p. 73, 1999.
54. Berger, I.; Kang, C. H.; Sinha, N.; Wolters, M.; Rich A. *Acta Cryst D* 1996, 52, 465–468.
55. Otwinowski, Z.; Minor, W. *Methods Enzymol* 1997, 276, 307–326.
56. Weeks, C. M.; Miller, R. *J Appl Cryst* 1999, 32, 120–124.
57. Weeks, C. M.; Miller, R. *Acta Cryst D* 1999, 55, 492–500.
58. Berman, H. M.; Zardecki, C.; Westbrook, J. *Acta Cryst D* 1998, 54, 1095–1104.
59. Brünger, A. T. *Crystallography & NMR System (CNS, Version 0.3)*; Yale University, New Haven, CT, 1998.
60. Parkinson, G.; Vojtechovsky, J.; Clowney, L.; Brünger, A. T.; Berman, H. M. *Acta Cryst D* 1996, 52, 57–64.
61. Brünger, A. T. *Nature* 1992, 355, 472–475.
62. Cambillau, C.; Roussel, A. Turbo Frodo, Version OpenGL.1, Université Aix-Marseille II, Marseille, France, 1997.
63. Sheldrick, G. M.; Schneider, T. R. *Methods Enzymol* 1997, 276, 319–343.
64. Westhof, E. *Int J Biol Macromol* 1987, 9, 186–191.
65. Shakked, Z.; Guzikevich-Guerstein, G.; Frolow, F.; Rabinovich, D.; Joachimiak, A.; Sigler, P. B. In *Structural Biology: The State of the Art*; Sarma, R. H., Sarma, M. H., Eds.; Adenine Press: Schenectady, NY, 1994; Vol 1, pp 199–216.
66. Guzikevich-Guerstein, G.; Shakked, Z. *Nature Struct Biol* 1996, 3, 32–37.
67. Stec, B.; Zhou, R.; Teeter, M. M. *Acta Cryst D* 1995, 51, 663–681.
68. Bingman, C.; Li, X.; Zon, G.; Sundaralingam, M. *Biochemistry* 1992, 31, 12803–12812.
69. Harlow, R. L. *J Am Chem Soc* 1993, 115, 9838–9839.
70. Haran, T. E.; Shakked, Z.; Wang, A. H.-J.; Rich, A. *J Biomol Struct Dynam* 1987, 5, 199–217.
71. Brown, I. D.; Wu K. K. *Acta Cryst B* 1976, 32, 1957–1959.
72. Di Cera, E.; Guinto, E. R.; Vindigni, A.; Dang, Q. D.; Ayala, Y. M.; Wuyi, M.; Tulinsky, A. *J Biol Chem* 1995, 270, 22089–22092.
73. Nayal, M.; Di Cera, E. *J Mol Biol* 1996, 256, 228–234.
74. Lavery, R.; Sklenar, H. J. *J Biomol Struct Dynam* 1989, 6, 655–667.